Materials Today Bio 29 (2024) 101347

Contents lists available at ScienceDirect

Materials Today Bio

journal homepage: www.journals.elsevier.com/materials-today-bio

Metformin carbon dots enhance neurogenesis and neuroprotection in Alzheimer's disease: A potential nanomedicine approach

Jing Zhang [a], Xuehan Yang [a], Sushan Wang [a], Jianhua Dong [a], Meishuang Zhang [b], Ming Zhang [a,**], Li Chen [a,b,*]

[a] Department of Pharmacology, Nanomedicine Engineering Laboratory of Jilin Province, College of Basic Medical Sciences, Jilin University, Changchun, 130021, China
[b] School of Nursing, Jilin University, Changchun, 130021, China

ARTICLE INFO

Keywords:
CMCDs
Alzheimer's disease
Neural stem cells
Neurogenesis
Neuroprotection

ABSTRACT

Alzheimer's disease (AD) is characterized by progressive cognitive decline due to neuronal damage and impaired neurogenesis. Preserving neuronal integrity and stimulating neurogenesis are promising therapeutic strategies to combat AD-related cognitive dysfunction. In this study, we synthesized metformin carbon dots (CMCDs) using a hydrothermal method with metformin hydrochloride and citric acid as precursors. Notably, we found that CMCDs were significantly more effective than metformin in promoting the differentiation of neural stem cells (NSCs) into functional neurons under amyloid-beta (Aβ) conditions. Moreover, CMCDs fostered NSCs proliferation, enhanced neurogenesis, reduced Aβ deposition, and inhibited glial cell activation. We also examined neuronal structure by assessing Map2/NF-H/PSD95/SYN expression in the hippocampus, finding that CMCDs robustly strengthened neuronal structure. These results suggest that CMCDs can cognitive dysfunction in AD and promote the proliferation and neurogenesis of NSCs, as well as ameliorate neuronal injury. Hence, CMCDs emerge as promising candidates for AD therapy, demonstrating superior efficacy compared to metformin alone, and offering novel insights into small molecule drug interventions for AD.

1. Introduction

Alzheimer's disease (AD), a progressive neurodegenerative disorder, poses significant economic and social burdens [1,2] due to advancing neuronal damage, neuronal loss, and the accumulation of extracellular Aβ plaques and intracellular neurofibrillary tangles [3–5]. Existing clinical treatments offer only modest and temporary relief of symptoms without addressing the underlying neuropathology [6]. The absence of effective treatments has contributed to the increasing global prevalence of AD, especially as the aging population grows [7]. While multifactorial, neuronal damage and loss primarily contribute to memory impairment and cognitive decline in AD. Therefore, enhancing neuronal repair and promoting neurogenesis emerge as appealing strategies for AD therapy (see Scheme 1).

Neurogenesis—the formation of new neurons—continues throughout adulthood in certain brain regions, particularly the hippocampal dentate gyrus (DG) [8,9]. Adult hippocampal neurogenesis plays a critical role in certain forms of learning and memory [10,11], making it a promising target for AD therapy [12]. Likewise, addressing neuronal damage is crucial for preserving cognitive function by preventing neuron and synapse loss [13,14]. Developing small-molecule drugs to enhance neuronal repair and stimulate neurogenesis is an attractive strategy for AD therapy. However, traditional small-molecule compounds often face limitations in reaching sufficient brain concentrations to exert therapeutic effects [15,16]. This highlights the need for innovative therapeutic approaches.

Metformin, a widely used medication for type 2 diabetes, has demonstrated the ability to delay disease progression in animal models and clinical studies [17,18]. Additionally, metformin reduces mortality in patients with cardiovascular disease [19], though its benefits in diabetic populations are debated [20]. Metformin has also shown neuroprotective effects relevant to AD, including reducing Aβ production [21], inhibiting tau phosphorylation [22], enhancing hippocampal neurogenesis [23,24], alleviating neuroinflammation [25], and

* Corresponding author. Department of Pharmacology, College of Basic Medical Sciences, School of nursing, Jilin University, 126 Xin Min Street, Changchun, Jilin, 130021, China.
** Corresponding author. Department of Pharmacology, College of Basic Medical Sciences, Jilin University, 126 Xin Min Street, Changchun, Jilin 130021, China.
E-mail addresses: zhangming99@jlu.edu.cn (M. Zhang), chenl@jlu.edu.cn (L. Chen).

https://doi.org/10.1016/j.mtbio.2024.101347
Received 20 August 2024; Received in revised form 6 November 2024; Accepted 15 November 2024
Available online 16 November 2024

enhancing cognitive performance [25–27]. However, despite metformin's ability to cross the blood-brain barrier (BBB), its therapeutic effects in AD vary, possibly due to challenges in achieving adequate brain concentrations and high clearance rates.

Nanomedicine offers promising solutions for overcoming pharmacological barriers in AD treatment. Nanodrugs can effectively accumulate in the brain following systemic administration, leveraging enhanced permeability and retention effects [28,29]. Moreover, surface functionalization augments their ability to traverse biological barriers and reach target cells [30,31]. Carbon dots (CDs), in particular, hold unique advantages as nanomaterials, including ultra-small size (typically < 10 nm), high BBB penetration, excellent biocompatibility, stability, cellular uptake, and cargo delivery capabilities [32,33]. These properties make CDs ideal candidates for drug delivery to the brain, offering potential therapeutic effects in AD [34,35].

Previous studies have investigated the potential of CDs and other nanoparticles in AD treatment. For example, Anand et al. demonstrated that native PLGA, without any drug or agent conjugation, can reduce Aβ aggregation and toxicity and attenuate AD pathology in cell and animal models [36]. Rompicherla et al. found that intranasal delivery of rivastigmine-loaded liposomes was more effective in reversing memory deficits in AD rat models than oral rivastigmine and other intranasal formulations [37]. Zhou et al. developed amphiphilic yellow-emissive CDs as non-toxic nanocarriers for central nervous system drug delivery and as inhibitors of amyloid plaques [38]. Compared to these approaches, our study using CMCDs targets multiple pathological processes in AD simultaneously, potentially offering more substantial and lasting therapeutic benefits. CMCDs are easy to synthesize, demonstrate good biocompatibility, and show promise for clinical translation.

In conclusion, combining metformin with CDs is a novel nanomedicine approach for enhancing AD therapy. CMCDs offer the potential to overcome current limitations of metformin in AD treatment while leveraging the unique properties of CDs for targeted brain delivery. Compared to other nanomedicine strategies, CMCDs simultaneously address multiple pathological processes in AD, potentially providing synergistic therapeutic effects.

Building upon these insights, our present study synthesized CMCDs using metformin and citric acid, and, for the first time, assessed their impact on cognitive function in AD. *In vitro* experiments demonstrated that CMCDs promoted NSCs differentiation into functional neurons in an $A\beta_{1\text{-}42}$ oligomeric environment, laying the groundwork for neural network integration. *In vivo* experiments revealed that CMCDs administration attenuated neuroinflammation and Aβ deposition, thereby improving the brain microenvironment, fostering neurogenesis, preserving neuronal structure, and mitigating synaptic loss. CMCDs exhibited superior therapeutic efficacy for AD compared to metformin alone in both *in vivo* and *in vitro* settings. Our findings unveil new horizons for nanomedicine-centered small molecule drug therapy for AD by elucidating the effects of CMCDs on driving neurogenesis and neuronal repair.

2. Materials and methods

2.1. Chemicals

Metformin hydrochloride and citric acid (CA) were procured from Sigma Aldrich (MO, USA). DMEM/F12-Dulbecco's Modified Eagle Medium (DMEM/F12), penicillin-streptomycin, MEM Non-Essential Amino Acids, and B27 Supplement were obtained from Gibco (NY, USA). Basic fibroblast growth factor (bFGF) and epidermal growth factor (EGF) were sourced from Peprotech (NJ, USA), while the Cell counting kit-8 (CCK-8) was acquired from Bimake (Houston, USA). $A\beta_{1\text{-}42}$ monomer powder was obtained from GL Biochem Ltd. (Shanghai, China). Primary antibodies against Nestin, Sox2, Ki67, βIII-tubulin, Iba-1, GFAP, DCX, BrdU, NF-H, Map2, PSD95, and SYN were purchased from Abcam (MA, USA), and secondary antibodies from Proteintech (Wuhan, China). All chemicals, unless otherwise noted, were from Sigma Aldrich and used as received. Reagents not procured from Sigma Aldrich are analytical grade

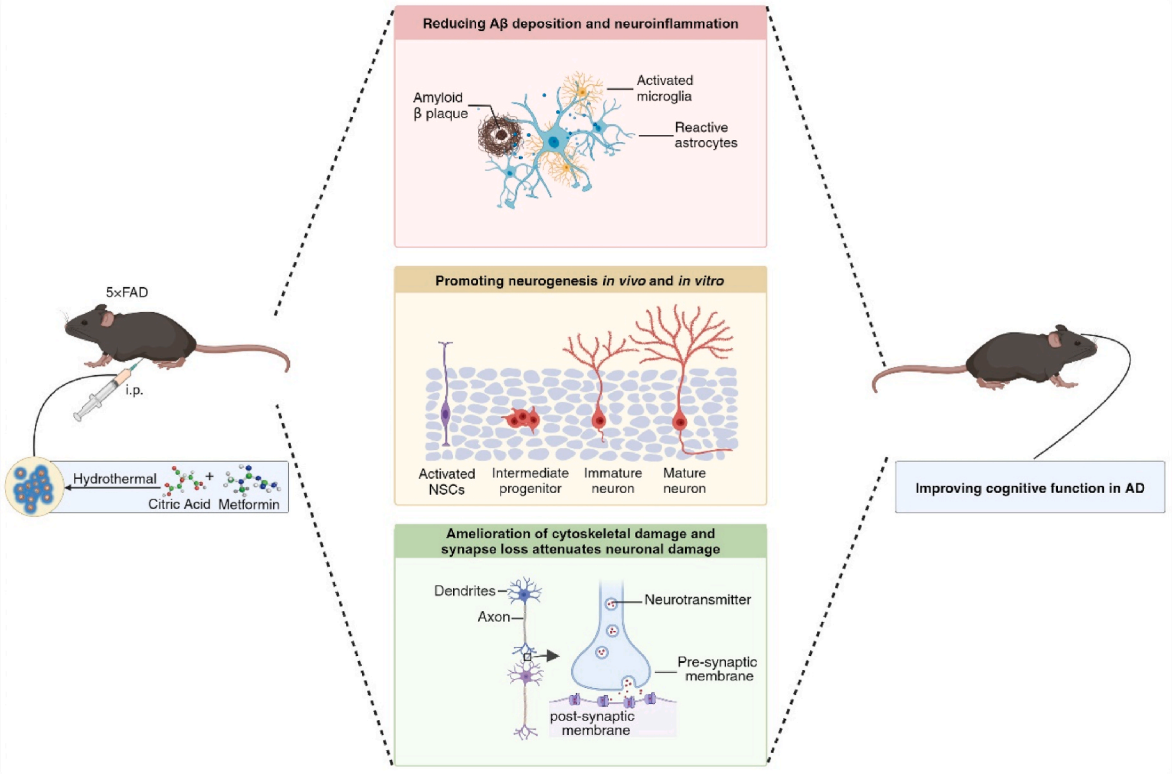

Scheme 1. Schematic illustrating the ability of CMCDs to enhance neurogenesis and neuroprotection in Alzheimer's disease (Created with BioRender.com) [CrossRef Exact].

and should be used as received.

2.2. Synthesis of CMCDs

CMCDs were synthesized by dissolving 33.124 mg of metformin hydrochloride in 10 mL of deionized water containing 10 mM citric acid. The resulting mixture was transferred to a Teflon-coated autoclave (Beijing Taida Technology Co. Ltd., Beijing, China) and heated at 180 °C for 8 h. After cooling to room temperature, the solution was filtered through a 0.22 μm membrane, followed by dialysis in deionized water for 48h using a dialysis bag (MWCO = 1000Da, Solarbio Company, Beijing, China), with water changes every 6 h. The final transparent yellow-brown CMCDs were lyophilized and stored for subsequent experiments.

2.3. Characterization of the CMCDs

Various analytical techniques were employed to characterize CMCDs. Transmission electron microscopy (TEM) was conducted using a Hitachi H-800 electron microscope (Tokyo, Japan) with a CCD camera, operating at an acceleration voltage of 200 kV. High-resolution TEM (HRTEM) analysis was performed with a JEM-2100F electron microscope (JEOL, Tokyo, Japan). Photoluminescence (PL) spectroscopy measurements were carried out on a Shimadzu RF-5301 PC spectrophotometer (Tokyo, Japan), while UV–vis absorption spectra were acquired using a 3100 UV–vis spectrophotometer (Shimadzu, Tokyo, Japan). Fourier transform infrared (FTIR) spectra were obtained using a Nicolet AVATAR 360 FTIR instrument (Madison, WI, USA). X-ray photoelectron spectroscopy (XPS) analysis was conducted using an ESCALAB MKII spectrometer (VG Scientific, UK) with Mg Kα excitation (1253.6 eV), with binding energy calibration based on C1s at 284.6 eV.

2.4. Preparation of $A\beta_{1\text{-}42}$ oligomers

To prepare the $A\beta_{1\text{-}42}$ oligomers, 1 mg of $A\beta_{1\text{-}42}$ monomer powder was fully dissolved in 220 μL of cooled hexafluoroisopropanol (HFIP) for 60 min at room temperature. The solution was then placed on ice for 10 min and transferred to a fume hood with the cap open to allow HFIP evaporation. Once air-dried, the resulting Aβ peptide film was dissolved in 44 μL of fresh anhydrous dimethyl sulfoxide (DMSO) to create a 5 mmol/L $A\beta_{1\text{-}42}$ solution. This was diluted to a final concentration of 100 μmol/L in phenol red-free DMEM/F12 medium, incubated at 4 °C for 24 h, and centrifuged at 4 °C for 10 min at 14,000 rpm. The supernatant containing the $A\beta_{1\text{-}42}$ oligomers was collected, aliquoted, and stored at −80 °C.

2.5. NSCs culture and identification

All animal procedures were approved by the Animal Research Committee of Jilin University, Changchun, China. E12-E14 fetal brain tissue from C57BL/6 mice (n = 6) was used to isolate NSCs. Meninges were removed, and brain tissue was diced into 1–2 mm^3 pieces in cold DMEM/F12 medium, followed by centrifugation at 500 rpm for 1 min to remove larger tissue fragments. The supernatant was further centrifuged at 800 rpm for 3 min to discard debris and cell membranes. The isolated cells were resuspended in growth media (DMEM/F12 supplemented with B27, bFGF (20 ng/mL), and EGF (20 ng/mL)) and filtered through a 75 μm cell strainer to create a single-cell suspension. Cells were then seeded in Nunc T25 culture flasks (5000 cells/cm^2) and incubated at 37 °C with 5 % CO_2, leading to neurosphere formation. Neurospheres were dissociated using Accutase, plated on poly-D-lysine (PDL) and laminin-coated plates, and confirmed using antibodies against NSCs-specific markers Nestin and Sox2, with Hoechst staining for nuclear visualization.

2.6. Differentiation and characterization of NSCs

To assess the differentiation potential of NSCs, cultures were grown without EGF and bFGF. After 14 days, immunofluorescent labeling was conducted using antibodies against glial marker GFAP and neuronal marker Map2, with Hoechst stain for nuclear labeling. To evaluate the effect of CMCDs on NSC differentiation, the differentiation medium was supplemented with metformin or CMCDs (at metformin-equivalent concentrations).

2.7. Cytotoxicity measurement

To assess CMCDs cytotoxicity, neurospheres in the logarithmic phase were digested with Accutase and seeded at a density of 1.0×10^4 cells per well onto treated 96-well plates. After 24h, the plates were washed with PBS, and the differentiation medium was supplemented with various concentrations of metformin and CMCDs (at equivalent metformin concentrations) every 3 days. Following 1, 7, 14, and 21 days of incubation, 10 μL of CCK-8 solution was added to each well and incubated for 4h. Absorbance was measured at 450 nm, with untreated cells serving as controls (100 % viability).

2.8. Neuroprotective effects of CMCDs

To assess the neuroprotective effects of CMCDs, NSCs were co-incubated with various concentrations of CMCDs for 4h. After washing twice with PBS, differentiation medium with or without CMCDs was added along with $A\beta_{1\text{-}42}$ Oligomers (10 μM), followed by incubation at 37 °C for 3d to evaluate cell viability using the CCK-8 kit.

2.9. RT-qPCR

Differentiated cells were harvested using the RNAeasyTM Animal RNA Isolation Kit with Spin Column (Beyotime Biotechnology, Shanghai, China) after 7 days in differentiation medium containing $A\beta_{1\text{-}42}$ oligomers (10 μM) with or without the addition of CMCDs. Total RNA was extracted and cDNA was synthesized using the TransScript® First-Strand cDNA Synthesis SuperMix (TransGen Biotech, Beijing, China). RT-qPCR was performed using the SYBR Green I Mix (Roche, Shanghai, China) and QuantStudio 3 Real-Time PCR System (Thermo Fisher Scientific Ltd., Waltham, MA, USA) to determine the expression of neurogenic genes including DCX, Map2, βIII-tubulin, and GFAP, with Actin serving as an internal control. Please refer to Table S1 for the list of primers used.

2.10. Neurite outgrowth assay

The differentiation medium was supplemented with CMCDs (1.58 μg/mL) and metformin(1 μg/mL) without EGF and bFGF. After 4h, $A\beta_{1\text{-}42}$ oligomers at 10 μM were added, and co-cultivation was continued for 8 days. Immunofluorescent staining with βIII-tubulin and GFAP was performed to determine the count, length, and branching points of neurons. Neurite lengths measured were required to be at least twice as long as the soma.

2.11. Intraperitoneal injection of CMCDs in 5 × FAD

In this study, 5 × FAD mice, which mimic key aspects of Alzheimer's disease (AD) pathology, were used to investigate the effects of CMCDs on AD-related neurogenesis and cognitive impairment. The 5 × FAD model is characterized by amyloid plaque formation, neuroinflammation, synaptic dysfunction, cognitive deficits [39], and impaired adult hippocampal neurogenesis [40]. The model recapitulates several key aspects of human AD pathology provides a suitable platform for exploring AD mechanisms and evaluating potential therapeutic interventions.

Five-month-old male 5 × FAD and wild-type (WT) mice were sourced

from Shanghai Southern Model Biotechnology Co., Ltd. Following a week of acclimation, mice were divided into four groups (n ≥ 6 per group): WT (saline control), 5 × FAD (saline control), 5 × FAD (Met-CA mix: 220 mg of metformin hydrochloride and 130 mg citric acid in 10 mL saline, 350 mg/kg intraperitoneal injection), 5 × FAD (CMCDs: 350 mg/kg intraperitoneal injection). The Met-CA mix group was included to differentiate the effects of the physical mixture from the synthesized CMCDs. Injections were administered for three weeks, and mice were monitored weekly for weight and behavioral performance.

2.12. BrdU injection

To trace cell survival and differentiation, mice received twice-daily intraperitoneal injections of BrdU (50 mg/kg) starting on day 17 for five consecutive days.

2.13. Morris water maze (MWM) experiment

To assess learning and memory, the MWM test was conducted three weeks post-treatment. A pool (diameter 1.1m) was filled with non-toxic titanium liquid at 22 ± 1 °C, refreshed daily. Over a 6-day hidden platform trial, mice were trained to locate a submerged platform. Training consisted of four 60-s trials per day, spaced 1 h apart, with mice allowed to remain on the platform for 15 s if located within the time limit.

To test spatial memory, the platform was removed 24h after the final training session, and each mouse swam freely for 60 s. The time taken to find the original platform location, swimming speed, and number of times the original platform area was crossed were recorded. Mice spending more time in the target quadrant were considered to demonstrate superior spatial memory.

2.14. Nissl staining

After the MWM test, mice were anesthetized, perfused, and their brain and visceral tissues fixed, dehydrated, and embedded in paraffin. Hippocampal sections (5 μm) were stained with a Nissl Staining Kit (Beyotime Biotechnology, Shanghai, China) to visualize Nissl bodies in neuronal cytoplasm. Sections were stained at 37 °C for 10 min, rinsed with water, dehydrated in ethanol, and cleared in xylene.

2.15. Hematoxylin and eosin staining

Deparaffinized, rehydrated sections of brain and visceral tissues (heart, liver, kidney, lung, spleen) were stained with hematoxylin for 5 min, washed, differentiated in 1 % hydrochloric acid-alcohol for 5 s, rewashed, then stained with 0.5 % eosin for 2 min. Sections were dehydrated through an ethanol gradient, cleared in xylene, and sealed with neutral gum.

2.16. Immunofluorescence

Paraffin-embedded sections were initially subjected to deparaffinization and subsequent rehydration. The samples were then rinsed with distilled water and heated in 10 mM sodium citrate buffer (pH 6.0) (Beyotime) for 20min at 95 °C. After cooling the sections to room temperature (RT), they were permeabilized for 20min with 0.4 % Triton X-100 (Beyotime), blocked with 5 % sheep serum in PBS for 1h, and incubated with primary antibody overnight at 4 °C followed by fluorescently labeled secondary antibody for 1h at RT. The nuclei of the cells were stained with DAPI (Beyotime) before mounting the sections in an anti-fading mounting solution (Beyotime).

2.17. Immunohistochemistry

Procedures for antigen retrieval and permeabilization were as described in the "Immunofluorescence" section. To deactivate endogenous peroxidase, sections underwent a 20min incubation with 3 % H_2O_2. Subsequently, the sections were blocked with 5 % sheep serum in PBS for 1 h and then incubated with the primary antibody overnight at 4 °C. Following this, sections were incubated with horseradish peroxidase-conjugated secondary antibodies for 1 h at room temperature (RT), followed by color development with DAB and counterstaining with hematoxylin. Finally, neutral resin was used to seal the sections.

All histologic sections were scanned using a digital slide scanner (3DHISTECH, Hungary), and images were captured using CaseViewer 2.4.

2.18. Statistical analysis

Data are expressed as mean ± SD unless otherwise specified. Statistical significance among groups was assessed using one-way analysis of variance (ANOVA) followed by a Tukey post-hoc test. A threshold of $p < 0.05$ was considered statistically significant. Statistical analysis was performed using GraphPad Prism software (GraphPad Software Inc., San Diego, CA, USA).

3. Result and discussion

3.1. Characterization of CMCDs

The preparation of CMCDs was conducted as outlined in the experimental section (Fig. 1A). Typically, carbon dots are formed through condensation, polymerization, and carbonyl dehydration [41,42], resulting in graphitic carbon nuclei with functional groups on their surfaces. We hypothesize that an amide bond forms between the amine group of metformin and the carboxyl group of CA, leading to polyamide formation. Upon further heating, these polymers undergo carbonation, ultimately forming CMCDs. To achieve more uniform-sized CMCDs, a filtered and dialysis solution was prepared. Subsequently, the morphology characteristics of the CMCDs were examined using TEM and HRTEM. Fig. 1B depicts a TEM image of uniformly dispersed CMCDs without aggregation. The HRTEM image reveals well-resolved lattice planes with an inter-lattice spacing of ~0.21 nm. The nano-size of CMCDs facilitates their access to cells and enhances their pharmaceutical functions, with an average diameter of 2.95 nm (Fig. 1C).

The UV–Vis absorption spectrum of metformin in aqueous solution exhibits a characteristic absorption peak at 239 nm. Following hydrothermal treatment, another peak at 338 nm is observed in the UV–Vis absorption spectrum of CMCDs, indicating that the PL originates from the heterostructure between surface groups and the carbon core (Fig. 1D). The 200–400 nm absorption bands in nitrogen-doped carbon dots are attributed to the n-π* electronic transition of C=O and the π-π* electronic transition of the conjugated structure of nitrogen and carbon [43]. PL spectra of CMCDs are consistent with UV–visible absorption characteristics, with excitation spectra at 360 nm and an optimal emission wavelength of 450 nm (Fig. 1E).

FTIR was utilized to further investigate the chemical structure and surface functional groups of CMCDs. The FTIR spectrum of CA (Fig. 1F) shows the O-H stretching vibration at 3200-3500 cm^{-1} and the C=O stretching vibration at 1700-1750 cm^{-1}, indicating the presence of hydroxyl and carboxyl groups conducive to dehydration and carbonization. Metformin exhibits N-H stretching vibrations at 3368 and 3298 cm^{-1}, as well as C=N stretching vibrations at 1575 and 1626 cm^{-1} (Fig. 1F). The presence of amine groups in metformin, in conjunction with citric acid hydroxyl/carboxyl groups, provides the possibility that CMCDs can be dehydrated, condensed, and carbonated afterward [44]. The FTIR spectrum of CMCDs displays O-H/N-H stretching vibrations at 3000-3500 cm^{-1}. Peaks at 1670 and 1565 cm^{-1} are attributed to C=O and C=N/C=C stretching vibrations, respectively. These analyses indicate that CMCDs contain hydroxyl, amine, and carboxyl groups, as well as possible amide bonds (Fig. 1F).

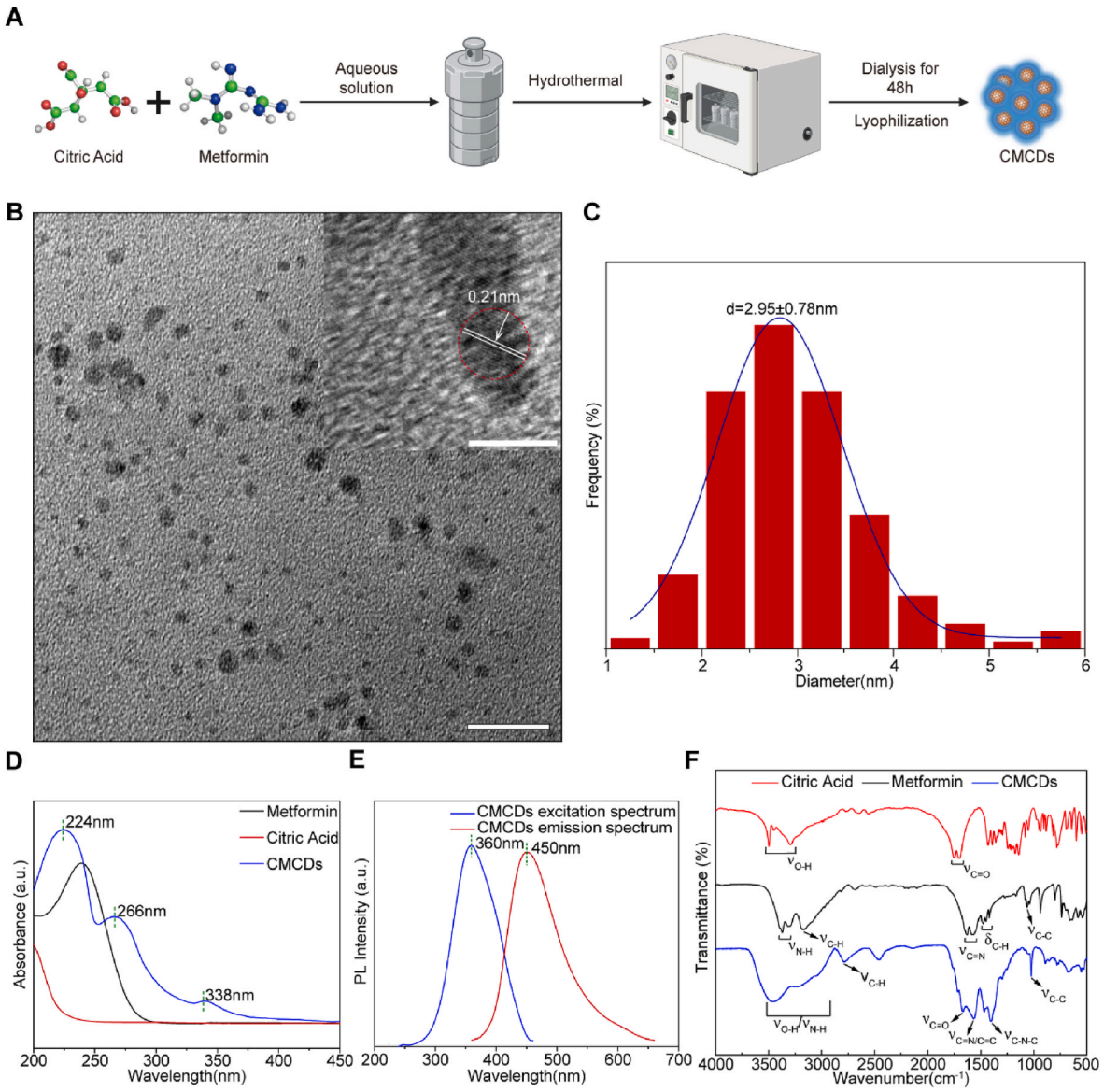

Fig. 1. Characterization of CMCDs. (A) Schematic illustration of the synthetic procedure of CMCDs (Created with BioRender.com). (B) TEM image (Scale bar: 20 μm) and HRTEM image (Scale bar: 5 μm) of CMCDs. (C) The size distributions of CMCDs. (D) UV–vis absorption spectra of CA (red), metformin (black), and CMCDs (blue). (E) The excitation spectrum (blue) and emission spectrum (red) of CMCDs. (F) FTIR spectra of CA (red), metformin (black), and the as-prepared CMCDs (blue)

XPS experiments were conducted to further investigate the surface functional groups of CMCDs. Fig. S1 shows the XPS spectra for the C1s, N1s, and O1s of CMCDs. The C1s spectra (Fig. S1A) reveal four peaks: O-C=O (289.3 eV), O=C-N (287.8 eV), C-O (285.9 eV), and C-C (284.67 eV), supporting the amination of the citrate carboxyl group in citric acid. The N1s XPS spectra of CMCDs exhibit two peaks, the C-N peak at 401.1 eV and the C=N peak at 399.7 eV (Fig. S1B). Similarly, the O1s XPS spectra of CMCDs display two peaks, C-O at 532.7 eV and N-C=O at 531.4 eV. Fig. 1F and Fig. S1 demonstrate that CA and metformin form CMCDs via an amidation reaction, with the surface retaining the pharmacophoric moiety of both. Based on these findings, we hypothesize that the pharmacological effects of CMCDs remain comparable to those of metformin and citric acid.

3.2. *Differentiation and neuroprotection of NSCs by CMCDs in the presence of $A\beta_{1\text{-}42}$ oligomers*

NSCs were isolated from embryonic mouse brains (E12–E14) and cultured according to established protocols [45,46]. By the 3rd day of culture, the cells had aggregated into neurospheres with notable refractive properties, as shown in Fig. S2A. By the7th day, these neurospheres reached diameters of approximately 100–150 μm (Fig. S2B), indicating the need for passaging to prevent central necrosis. The protocols detailed in Figs. S3A and S4A were used to assess NSCs and their differentiation capacity. As illustrated in Fig. S3B, 90 % of the neural stem monocytes and neurospheres express Nestin and SOX2, well-established markers of NSCs [47]. Figs. S4B and S4C demonstrate the differentiation potential of NSCs into astrocytes and neurons, respectively. The isolated and cultured NSCs exhibited high levels of purity and robust differentiation capabilities, thus affirming their suitability for subsequent investigations.

To determine the optimal dose for NSCs differentiation experiments, we assessed the effects of metformin and CMCDs on differentiated NSCs over 1, 7, 14, and 21 days. CCK-8 assay results indicated no significant reduction in the viability of differentiated NSCs compared to controls, even at high CMCDs concentrations (15.8 μg/mL, equivalent to 10 μg/mL of metformin) over 1–7 days (Fig. S5). However, at a dose of 1 μg/mL, metformin reduced cell viability by 14.5 % by day 21 (Fig. S6),

suggesting that CMCDs have superior biocompatibility, which is advantageous for biological applications. Additionally, after 14 days of treatment with 1 μg/mL metformin or 1.58 μg/mL CMCDs (equivalent to 1 μg/mL metformin), there were no notable changes in NSCs differentiation morphology compared to the control group (Fig. S7).

To identify the optimal concentrations of CMCDs and metformin for further experiments, we tested various CMCDs concentrations for their effects on neuronal differentiation and survival in NSCs-derived neurons exposed to Aβ1-42 oligomers. As shown in Figs. S8 and 1.58 μg/mL CMCDs significantly upregulated neuronal markers and downregulated astrocyte markers. Additionally, this concentration notably reduced apoptotic cells (Fig. S9). Based on these findings, along with CCK-8 assay

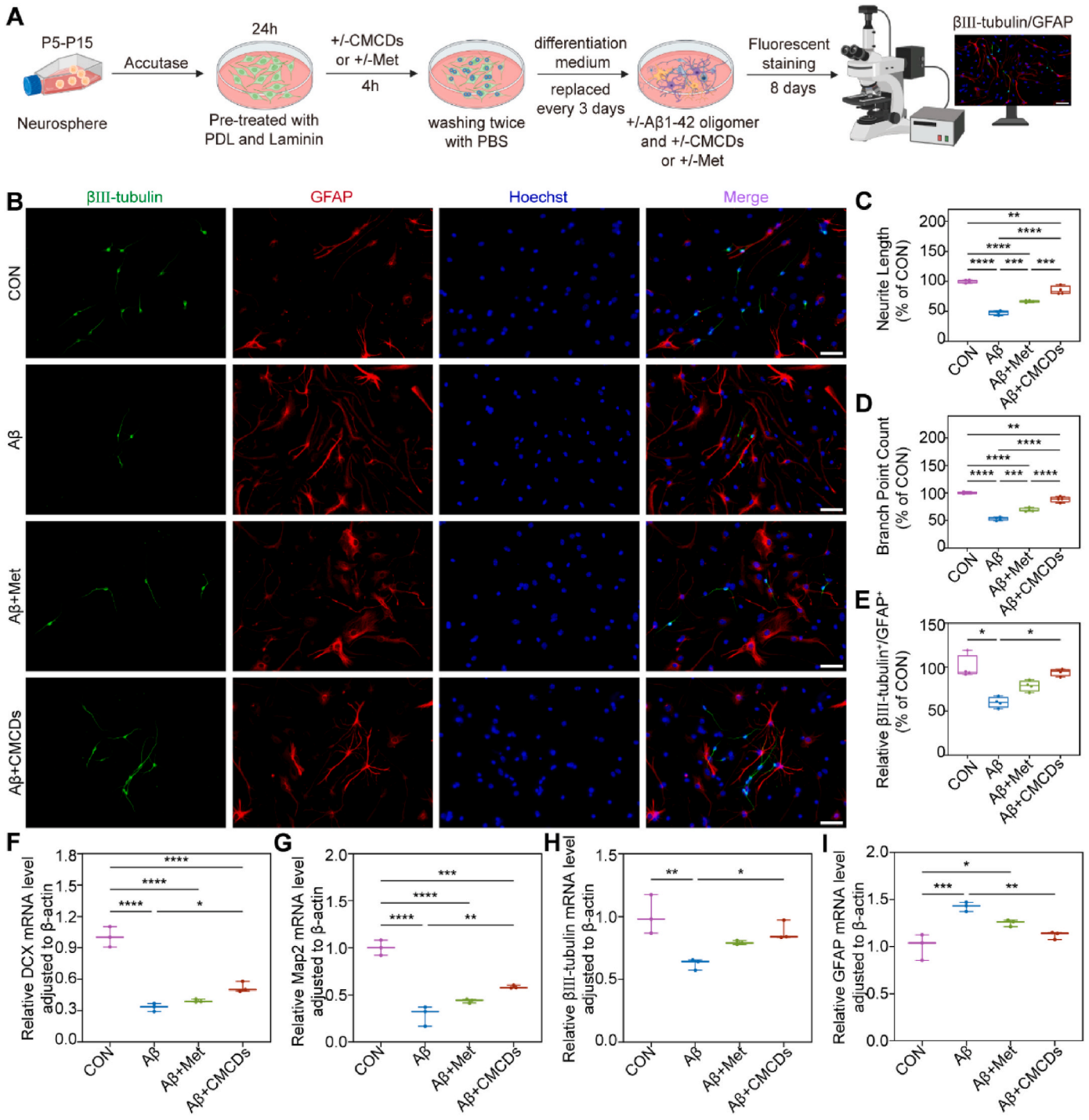

Fig. 2. Effects of CMCDs on NSCs differentiation and maturation under $A\beta_{1\text{-}42}$ oligomer exposure. (A) Schematic illustration of NSCs differentiation in response to various treatments under $A\beta_{1\text{-}42}$ aggregation (Created with BioRender.com). (B) NSCs differentiated for 8 days were examined to assess the impact of treatments on neuronal differentiation in the presence of $A\beta_{1\text{-}42}$ aggregation. Ten images were captured from random fields in each group (Scale bar:50 μm). (C) Neurite outgrowth was determined at DIV 8 using the NIH Image J plugin simple neurite tracer. (D) Branch numbers. (E) Neuron/astrocyte number ratio were quantified using the same images. (mean ± SD, n = 4, values were analyzed by one-way ANOVA with Tukey's posttest, *p < 0.05, **p < 0.01, ***p < 0.001, ****p < 0.0001). $A\beta_{1\text{-}42}$ aggregation leads to impaired neuronal differentiation due to the reduced expression of neuronal genes (F–H: DCX, Map2, and βIII-tubulin) and (I) increased expression of astrocytes. (mean ± SD, n = 3, values were analyzed by one-way ANOVA with Tukey's posttest, *p < 0.05, **p < 0.01, ***p < 0.001, ****p < 0.0001).

results, we selected 1.58 μg/mL CMCDs (equivalent to 1 μg/mL metformin) as the optimal dose for subsequent differentiation experiments.

To determine whether CMCDs could also ameliorate the neuronal differentiation defects in NSCs under $A\beta_{1-42}$ oligomers, we employed βIII-tubulin^{+}/GFAP $^{+}$ immunofluorescence to assess the neuronal differentiation in NSCs under the influence of $A\beta_{1-42}$ oligomers, in the presence of metformin and CMCDs. As shown in Fig. 2B, metformin treatment increased βIII-tubulin^{+} cells and reduced GFAP^{+} cells; however, these changes were not statistically significant compared to the Aβ group. In contrast, the CMCDs-treated group showed a significant increase in the βIII-tubulin^{+}/GFAP^{+} ratio compared to the Aβ group (Fig. 2E). This suggests that CMCDs, unlike metformin, effectively improved neuronal differentiation deficits in NSCs exposed to $A\beta_{1-42}$ oligomers. Furthermore, CMCDs notably upregulated βIII-tubulin expression while downregulating GFAP expression (Fig. 2H–I).

A crucial factor in treating neurodegenerative diseases with NSCs is their differentiation into mature, functional neurons [48]. A defining characteristic of mature neurons is the development of neurite outgrowths, essential for sensing neurotransmitter signals [49]. As shown in Fig. 2C, both metformin and CMCDs increased neurite length compared to the Aβ group; however, metformin did not restore neurite length to control levels. In Fig. 2D, both metformin and CMCDs significantly enhanced neurite branching compared to the Aβ group, with CMCDs exhibiting a greater effect than metformin. Collectively, these results indicate that CMCDs have a higher efficacy than metformin in facilitating NSCs differentiation into mature neurons in the presence of $A\beta_{1-42}$ oligomers.

The enhanced efficacy of CMCDs over metformin alone may be attributed to several factors, including improved BBB penetration, enhanced cellular uptake, and the controlled release of the therapeutic payload. The nanoscale size and surface properties of CMCDs likely facilitate their interaction with biological barriers and cellular

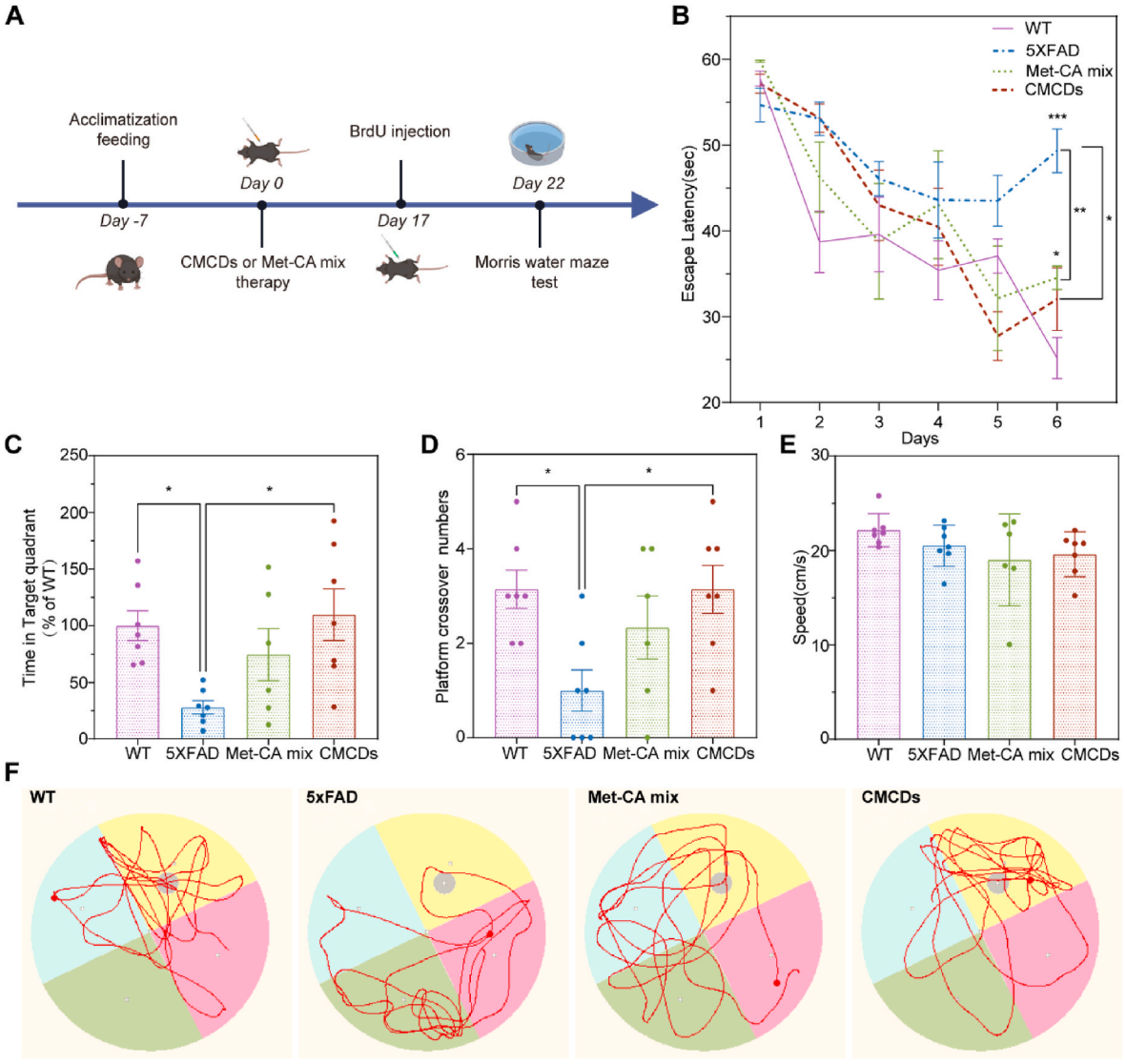

Fig. 3. CMCDs rescue cognitive deficits in 5 × FAD mice. Three weeks of treatment with Met-CA mix and CMCDs (350 mg/kg) was administered to 5 × FAD mice aged 5 months. As controls, WT mice and 5 × FAD mice treated with normal saline, respectively, served as normal and model controls. Beginning on the 17th day, all mice were injected intraperitoneally twice daily with BrdU (50 mg/kg) for five days. (A) Schematic illustration of the experimental setup for assessing cognitive function with CMCDs and the MWM experiment in 5 × FAD mice (Created with BioRender.com). (B) The escape latency of the MWM navigation experiment. (mean ± SEM, n ≥ 6, values were analyzed by two-way repeated ANOVA, *p < 0.05, **p < 0.01, ***p < 0.001). (C) The percentage of time spent in the quadrant where the escape platform used to be located. (D) Frequency of traversing the platform's location during the probe trial. (E) Swimming velocity of each group during the probe test. (C–E: mean ± SD, n ≥ 6, values were analyzed by one-way ANOVA with Tukey's posttest, *p < 0.05). (F) Representative traces of mouse navigation during the 60-s probe trial to locate the escape platform.

membranes, increasing bioavailability and enabling targeted brain delivery. Additionally, the carbon dot nanocarrier may provide sustained release of metformin, potentially amplifying its therapeutic effects. Future studies should focus on developing novel nanomedicine strategies that target multiple pathological facets of AD, such as neurogenesis, neuroinflammation, and amyloid-beta deposition.

It is noteworthy that the NSCs used in this study were isolated from embryonic mouse brains and cultured *in vitro*. While these cells provide a valuable model for examining the effects of CMCDs on neurogenesis and differentiation, they may not fully replicate the behavior and characteristics of adult neural stem/progenitor cells, which exist in a complex microenvironment *in vivo* and are influenced by various physiological cues. To address this limitation, we validated our findings *in vivo* using the 5 × FAD mouse model.

3.3. In vivo CMCDs exhibited enhanced cognitive flexibility

To evaluate whether CMCDs improve cognitive function in 5 × FAD transgenic mice, the Morris water maze (MWN) experiment was conducted in accordance with Fig. 3A. On the sixth day of training (Fig. 3B), the escape latency of mice in the 5 × FAD group was longer than that in the WT group, indicating cognitive deficits in the 5 × FAD mice. Both the CMCDs group and the Met-CA mix group showed reduced escape latency in the 5 × FAD mice, with the CMCDs group demonstrating a significant reduction, suggesting that CMCDs notably improved cognitive function in these mice.

To further assess memory capacity, we measured the time spent in the target quadrant and the number of platform location crossings in a spatial probe trial with the platform removed. Remarkably, CMCDs mitigated cognitive deficits in the 5 × FAD mice, whereas the Met-CA mix did not significantly affect learning or memory (Fig. 3C–F). In conclusion, CMCDs effectively ameliorate cognitive dysfunction in the 5 × FAD mouse model. This anti-dementia effect may be attributed to structural modifications during CMCD formation, which likely enhance their uptake and retention in the brain.

3.4. CMCDs ameliorated neural proliferation and neurogenesis deficits in the DG of 5 × FAD mice

Neurogenesis, the fundamental process through which neural precursor cells differentiate into neurons, is indeed profoundly impaired in AD [50]. The impaired neurogenesis observed in AD may contribute to cognitive deficits, highlighting the importance of investigating potential therapeutic strategies that stimulate neurogenesis. To explore whether CMCDs improve cognitive function by enhancing neurogenesis in the DG of 5 × FAD mice, we first examined the safety of CMCDs in 5 × FAD mice and then tested the expression of relevant markers associated with neurogenesis, including Ki67 for cell proliferation, Nestin for neural stem cells/precursor cells, and DCX/BrdU for newborn neurons.

The results are shown in Fig. S10, where histological examination of the major organs in the different treatment groups did not reveal any pathological changes. We then found that the proliferation of $Ki67^+$ and $Nestin^+$ cells were significantly decreased in the 5 × FAD group compared to the WT group. In contrast, there was no significant difference in the expression in the Met-CA mixed group compared to the 5 × FAD group. However, the expression was significantly elevated in the CMCDs group compared to the 5 × FAD group (Fig. 4A–D). Similarly, there was a statistically significant difference in the expression in the CMCDs group compared to the Met-CA mixed group.

To determine whether the observed increase in progenitors and neuronal cells in the CMCDs group would lead to subsequent alterations in DG neurogenesis, the quantification of newborn neurons was performed using DCX^+ $BrdU^+$ staining. The results showed that the number of DCX^+, $BrdU^+$ and DCX^+ $BrdU^+$ cells in the DG was significantly decreased in the 5 × FAD group compared to the WT group (Fig. 4E–H). There was no significant difference in the number of positive cells in the Met-CA mixed group compared to the 5 × FAD group, while the positive cells were significantly higher in the CMCDs group. Similarly, the number of positive expressions was statistically significant in the CMCDs group compared to the Met-CA mixed group.

Furthermore, the ratio of βIII-tubulin$^+$ cells to $GFAP^+$ cells was notably increased in the CMCDs-treated group (Fig. 2E and 2H-I), indicating enhanced differentiation of developed neurons. This suggests that CMCDs-treated NSCs differentiate into more neurons under $A\beta_{1\text{-}42}$ oligomer conditions compared to the model control, demonstrating greater neurogenic potential. Overall, these findings suggest that CMCDs enhance the neurogenic potential of AD, both *in vitro* and *in vivo*.

3.5. CMCDs alleviated neuronal impairment in the hippocampus of 5 × FAD mice

The hippocampus in the brain is a key structure in the memory circuit, and its primary role is to be responsible for memory and learning functions [51]. As shown in Fig. S11, HE results revealed that hippocampal neurons in WT mice exhibited a normal structure, characterized by abundant cytoplasm, slightly rounded nuclei, and clear morphology. In contrast, neurons in the CA1 and CA3 regions of 5 × FAD mice displayed signs of atrophy in the cytoplasm and cytosol. Additionally, most neurons exhibited darkly stained cytoplasm and nuclei, along with irregular nucleus morphology. However, in both the Met-CA mix and CMCDs groups, the majority of neuronal structures appeared normal and clear, indicating a preservation of neuronal integrity. Furthermore, the CMCDs group exhibited better improvement in neuronal structure compared to the Met-CA mix group.

Nissl staining results (Fig. S11) depicted that brain regions encompassing CA1, CA3, and DG in WT mice exhibited a high density of neurons, indicative of healthy neuronal populations. Conversely, in 5 × FAD mice, the number of CA3 neurons was significantly reduced in 5 × FAD mice compared with WT mice. Upon treatment with Met-CA mix and CMCDs, there was an improvement of CMCDs in the number of neurons observed in the CA3 regions. Given the pivotal role of hippocampal neurons in memory formation and retrieval, the findings from Figs. S11 and S12 suggest that CMCDs have the potential to enhance both the structure and number of neurons in 5 × FAD mice. This implies a possible mitigation of neuronal loss and subsequent improvement in cognitive impairment associated with AD.

Neuronal impairment is an essential characteristic of AD and is intimately linked to the disease's onset and progression. The study utilized Map2 and NF-H staining to evaluate the protective effects of CMCDs on structural damage and cytoskeletal alterations in hippocampal neurons of 5 × FAD mice (Fig. 5A and E). The fluorescence intensity of NF-H in CA1, CA3, and DG of 5 × FAD mice was significantly reduced compared to that of WT mice (Fig. 5B–D). While the NF-H fluorescence intensity showed a non-significant increase in the Met-CA mix group compared to 5 × FAD mice, the CMCDs-treated mice exhibited significantly higher fluorescence intensity in CA1, CA3, and DG. There was no significant difference in fluorescence intensity between the Met-CA mix group and the CMCDs group. Regarding Map2 fluorescence intensity (Fig. 5F–H), similar trends were observed as with NF-H in WT and 5 × FAD group. Compared to the 5 × FAD group, the Met-CA mix group showed a non-significant improvement, whereas the CMCDs group significantly increased Map2 fluorescence intensity in CA1 and CA3, but not in the DG region. These findings suggest that CMCDs can effectively mitigate cytoskeletal damage in 5 × FAD mice, thereby enhancing cognitive function.

To further explore the beneficial effects of CMCDs on synaptic deficits induced by impairment, SYN (presynaptic vesicle protein) and PSD95 (postsynaptic density protein) staining were employed in the study to assess synaptic deficits (Fig. 6A and E). The results revealed a statistically significant decrease in the fluorescence intensity of SYN and PSD95 in hippocampal CA1, CA3, and DG in the 5 × FAD group

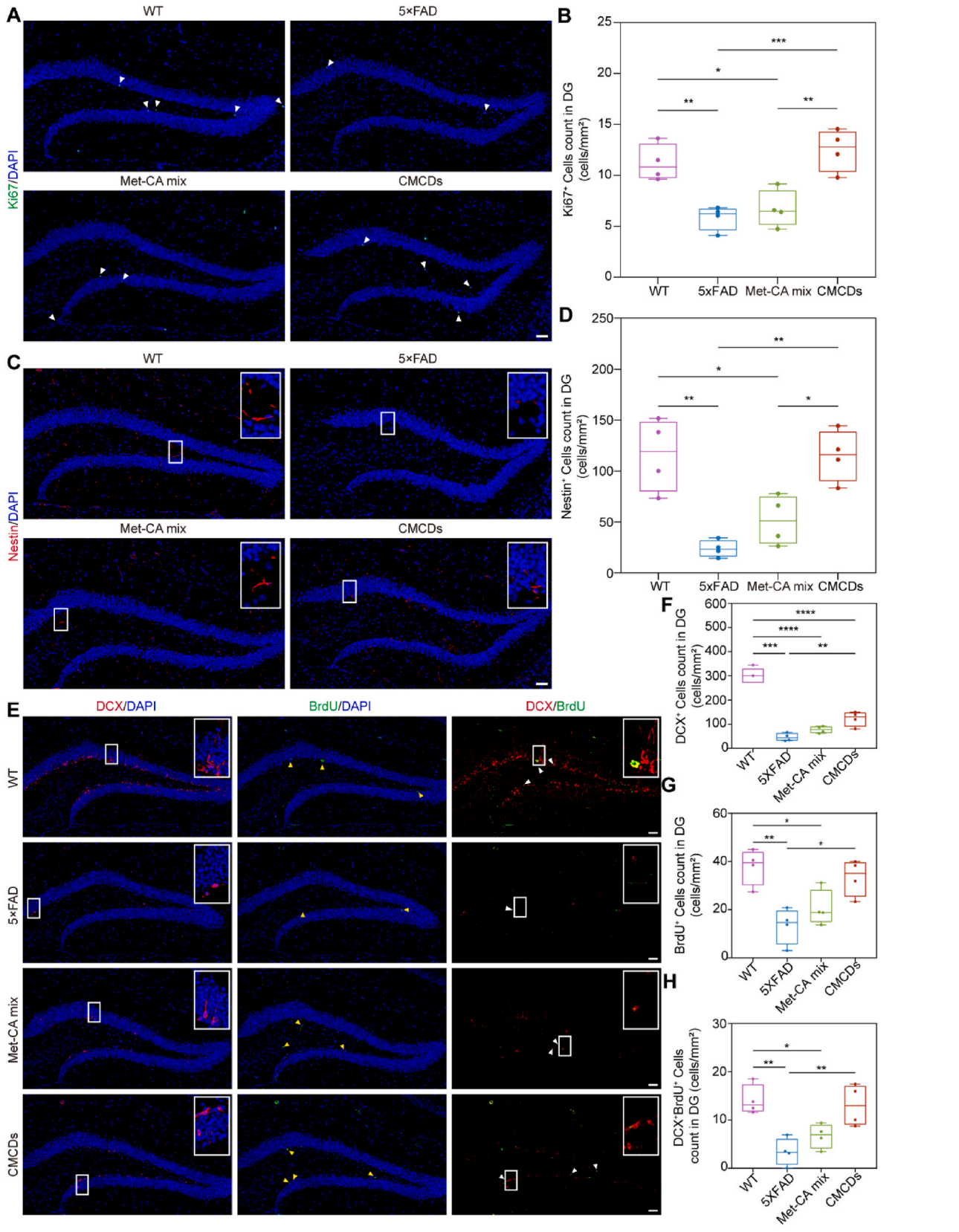

(caption on next page)

Fig. 4. CMCDs promoted neural proliferation and neurogenesis in the DG of 5 × FAD mice. To clarify the neurogenesis effects of CMCDs on the DG of 5 × FAD mice, we utilized immunofluorescence staining labeled with Ki67 (cell proliferation marker), Nestin (neural stem cells/neural precursor cell marker), DCX (neuronal precursor marker), and BrdU (cell proliferation marker) to double-stain and compare neurogenesis in the DG of the CMCDs group and the 5 × FAD group. (A) The effect of CMCDs on the number of Ki67-positive cells in the DG of 5 × FAD (Stained cells shown by white arrows. Scale bar: 50 μm). (B) Quantification of Ki67-positive cells in the DG of mice in the CMCDs group, as well as its respective normal and model controls. (mean ± SD, n = 4, values were analyzed by one-way ANOVA with Tukey's posttest, *p < 0.05, **p < 0.01, ***p < 0.001). (C) The impact of CMCDs on the quantity of Nestin-positive cells in the DG of 5 × FAD (White outlines enlarge stained cells. Scale bar: 50 μm). (D) Quantification of Nestin-positive cells in the DG of mice in the CMCDs group, along with the corresponding normal and model controls. (mean ± SD, n = 4, values were analyzed by one-way ANOVA with Tukey's posttest, *p < 0.05, **p < 0.01). (E) In each group of mice, DCX-, BrdU-, DCX- and BrdU-positive cells were detected in the DG (White contours represent enlarged stained cells, while yellow arrows denote stained cells. Scale bar: 50 μm). (F–H) Determining the number of DCX-(F), BrdU- (G), and DCX- BrdU-double-positive cells in the DG of mice in each group. (mean ± SD, n = 4, values were analyzed by one-way ANOVA with Tukey's posttest, *p < 0.05, **p < 0.01, ***p < 0.001, ****p < 0.0001).

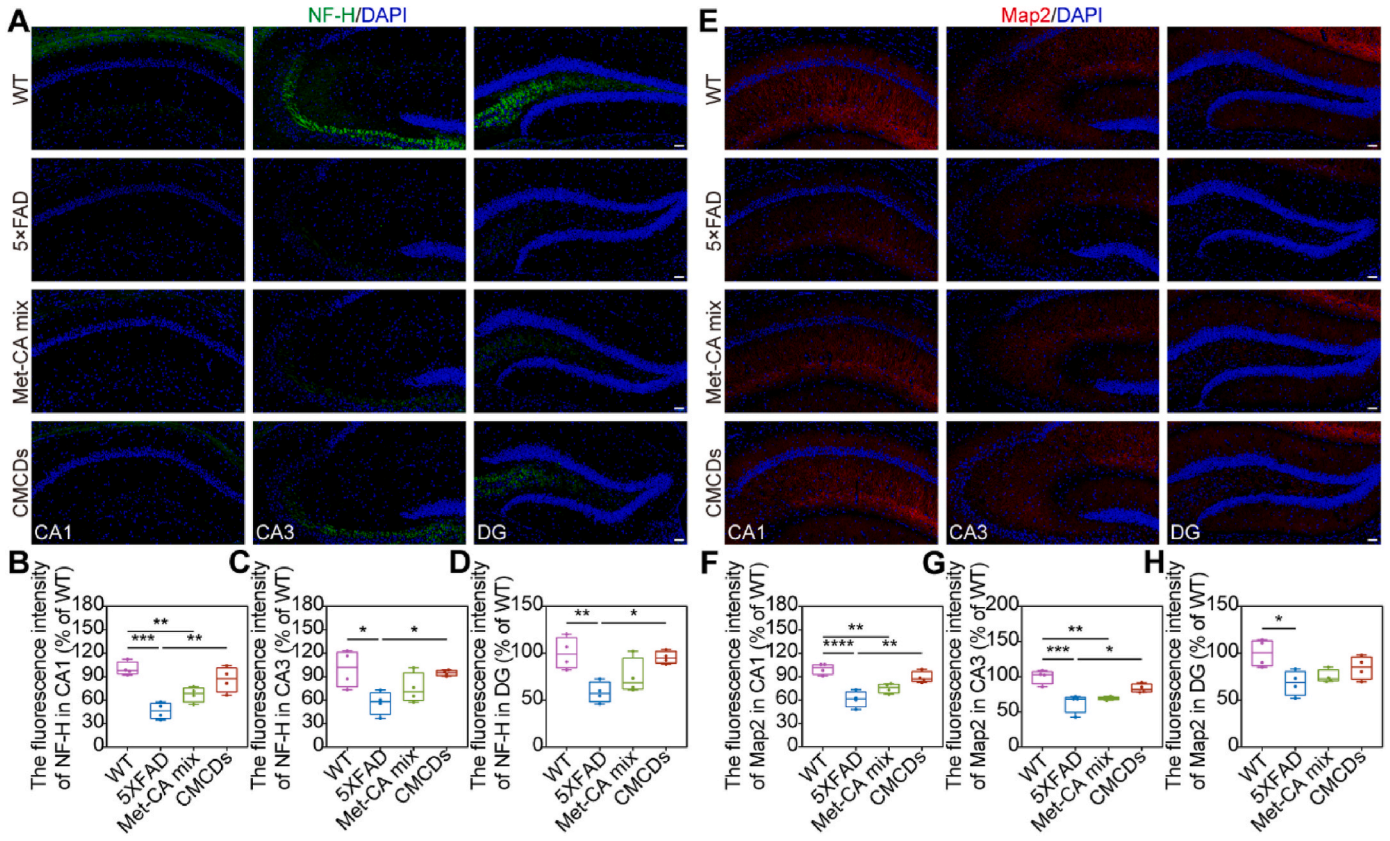

Fig. 5. CMCDs alleviated structural damage in the hippocampus of 5 × FAD mice. This study employed Map2 (a marker for dendritic spine density and dendritic morphology) and NF-H (a marker for axonal morphology and integrity) staining to assess the ameliorative effects of CMCDs on structural damage in hippocampal neurons of 5 × FAD mice. Scale bar: 50 μm. (A) The effect of CMCDs on axonal damage in the hippocampus of 5 × FAD mice. (B–D) The mean fluorescence intensity of NF-H in CA1, CA3, and DG of 5 × FAD mice. (E) The effect of CMCDs on dendritic damage in the hippocampus of 5 × FAD mice. (F–H) The mean fluorescence intensity of Map2 in CA1, CA3, and DG of 5 × FAD mice. (mean ± SD, n = 4, values were analyzed by one-way ANOVA with Tukey's posttest, *p < 0.05, **p < 0.01, ***p < 0.001, ****p < 0.0001).

compared to the WT group (Fig. 6B–D and 6F-H). While a statistically significant increase in PSD95 expression was observed in the Met group, it was limited to CA1 and CA3, with no significant improvement in DG expression, and there was no significant alteration in SYN expression. In contrast, in the CMCDs group, both PSD95 and SYN fluorescence intensities were significantly increased in all hippocampal regions except for SYN in the DG, which did not show significant improvement. These results suggest that CMCDs effectively prevented synaptic loss induced by 5 × FAD mice, leading to improved cognitive performance.

3.6. CMCDs reduced Aβ deposition and neuroinflammation in the brain of 5 × FAD mice

The study demonstrated that Aβ deposition alters neuronal function and impairs cognitive abilities in mouse models of AD [52], while metformin is effective in improving Aβ deposition and thus cognitive function. To further elucidate whether the cognitive enhancement by CMCDs is associated with reduced Aβ deposition, $A\beta_{1\text{-}42}$ antibody was employed to detect Aβ deposition in the brains of 5 × FAD mice. The results depicted in Fig. S13 indicate a significant increase in Aβ plaque area in the CA1, CA3, and DG regions in 5 × FAD group compared to the WT group. Both the Met-CA mix and CMCDs groups exhibited reduced Aβ deposition in CA1 and DG, with the reduction in Aβ deposition in CMCDs group being comparable to that of the Met-CA mix group. Notably, the reduction observed in the CMCDs group appeared stronger than that of the Met-CA mix group, despite no improvement in DG area.

Neuroinflammation plays a significant role in the pathology of neurodegenerative diseases, including AD [53,54]. To assess the impact of CMCDs on the glial response in the AD brain, immunofluorescence staining was conducted using antibodies against GFAP for astrocytes and Iba-1 for microglia in the brains of 5 × FAD mice (Figs. S14A and S15A). The fluorescence intensity of GFAP was elevated in the hippocampus of

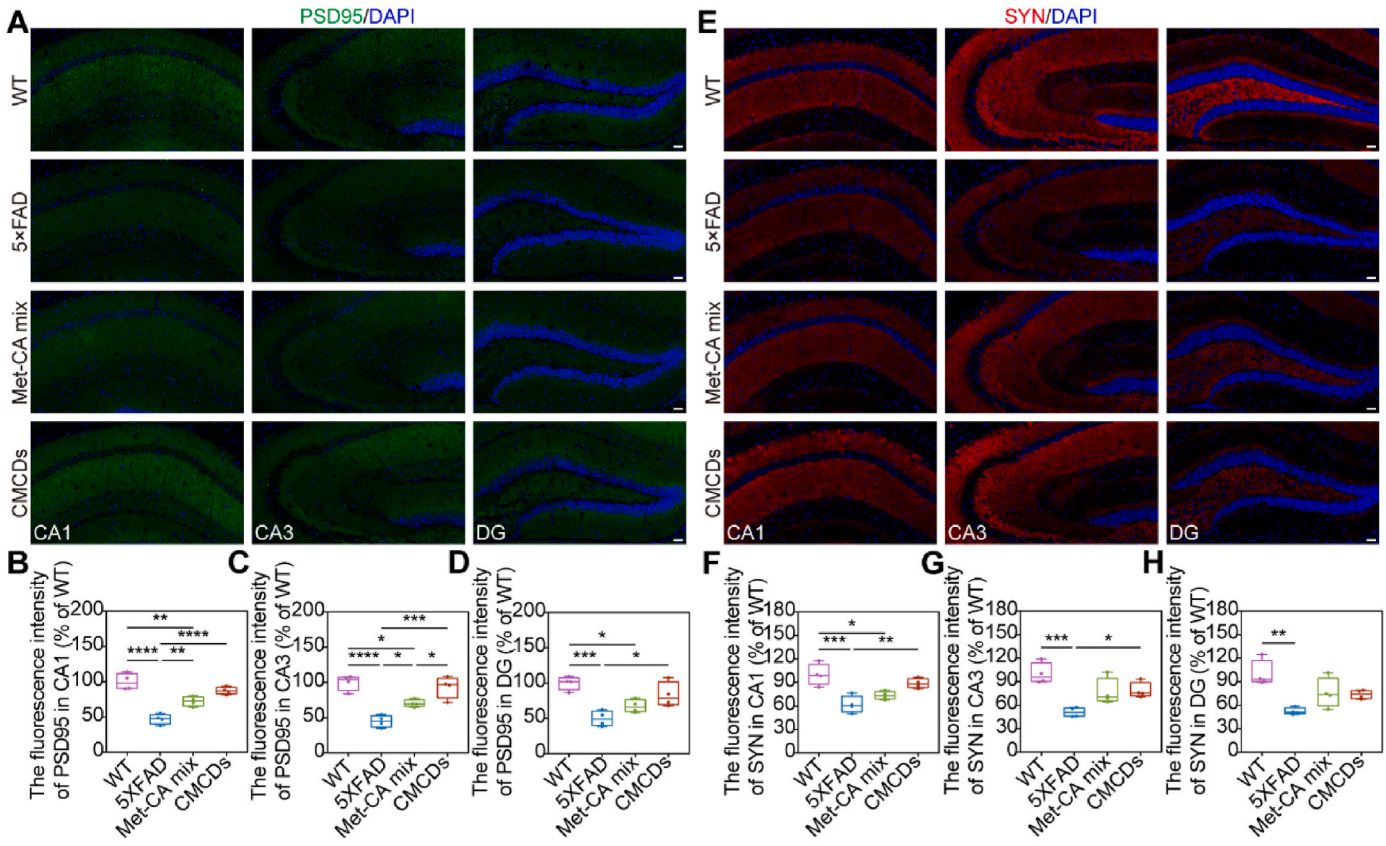

Fig. 6. CMCDs alleviated synaptic deficits in the hippocampus of 5 × FAD mice. This study utilized SYN (presynaptic vesicle protein) and PSD95 (postsynaptic density protein) staining for the ameliorative effect of CMCDs on synapse loss in hippocampal neurons of 5 × FAD mice. Scale bar: 50 μm. (A) The effect of CMCDs on postsynaptic density protein in the hippocampus of 5 × FAD mice. (B–D) The mean fluorescence intensity of PSD95 in CA1, CA3, and DG of 5 × FAD mice. (E) The effect of CMCDs on presynaptic vesicle protein in the hippocampus of 5 × FAD mice. (F–H) The mean fluorescence intensity of SYN in CA1, CA3, and DG of 5 × FAD mice. (mean ± SD, n = 4, values were analyzed by one-way ANOVA with Tukey's posttest, *p < 0.05, **p < 0.01, ***p < 0.001, ****p < 0.0001).

5 × FAD mice compared to WT mice (Figs. S14B–E). Conversely, the fluorescence intensity of Met-CA mix group was lower than that of 5 × FAD mice in CA1 and CA3. Notably, the fluorescence intensity in CA1, CA3, and DG in the CMCDs group was significantly lower than that in the 5 × FAD group, with the fluorescence intensity in CA1 being significantly lower than that in the Met-CA mix group. Consistent with the GFAP results, the fluorescence intensity of Iba-1 was increased in the hippocampus of 5 × FAD mice compared to WT mice (Figs. S15B–E). Additionally, the fluorescence intensity of Iba-1 in CA1, CA3, and DG of both Met-CA mix- and CMCDs-treated 5 × FAD mice was significantly lower than that of 5 × FAD mice. However, the fluorescence intensity in CMCDs group was significantly lower than that in Met-CA mix group only in the CA3 region, with decreased fluorescence intensity observed in CA1 and DG, although not statistically significant (Fig.S15B-E).

In summary, CMCDs elicit cognitive improvement by ameliorating neuroinflammation resulting from Aβ deposition and glial cell overactivation in the AD brain. These effects may be attributed to their modulation of the microenvironment in the AD brain.

While this study demonstrates the promise of CMCDs as a therapeutic nanomedicine for AD, it is essential to recognize the limitations of preclinical models. Although the 5 × FAD mouse model replicates key aspects of AD pathology, it does not fully capture the complexity of the human disease. Translating these findings to clinical applications will require further validation in additional preclinical models that more accurately mimic human AD, followed by clinical trials.

Furthermore, long-term safety, optimal dosing regimens, and the route of administration need to be explored. Investigating the potential for combination therapies with other AD drugs, as well as targeted delivery strategies to enhance the specificity and efficacy of CMCDs, is also critical. In addition, further studies are needed to elucidate the mechanisms underlying the neuroprotective and neurogenic effects of CMCDs, to fully assess their therapeutic potential in AD.

4. Conclusions

Compared to metformin, CMCDs demonstrated superior therapeutic efficacy in promoting neurogenesis and reducing neuronal damage in the context of AD. *In vitro*, CMCDs facilitated the efficient differentiation of NSCs into functional neurons even under the toxic conditions induced by $A\beta_{1\text{-}42}$ oligomers, laying the foundation for their potential integration into neural circuits. *In vivo*, CMCDs improved the brain's microenvironment in AD mice, promoting neurogenesis, repairing neuronal structural damage, and recovering lost synapses, which ultimately enhanced cognitive function.

CRediT authorship contribution statement

Jing Zhang: Writing – original draft, Validation, Data curation, Conceptualization. **Xuehan Yang:** Validation, Data curation. **Sushan Wang:** Data curation. **Jianhua Dong:** Validation, Data curation. **Meishuang Zhang:** Writing – review & editing, Writing – original draft, Funding acquisition. **Ming Zhang:** Writing – review & editing, Funding acquisition, Conceptualization. **Li Chen:** Writing – review & editing, Supervision, Funding acquisition, Conceptualization.

Notes

The authors declare no competing financial interest.

Ethics approval and consent to participate

All animal experiments were approved and performed following the guidelines of the Animal Research Committee of Jilin University, China.

Declaration of competing interest

The authors declare that they have no known competing financial interests or personal relationships that could have appeared to influence the work reported in this paper.

Acknowledgements

This work was supported by the Science and Technology Development Projects of Changchun (21ZY18), Interdisciplinary Integration and Innovation Project of JLU (JLUXKJC2021ZZ06), Education Department of Jilin Provincial (No. JJKH20231237KJ), Bethune Program of Jilin University (No. 2023B35).

Appendix A. Supplementary data

Supplementary data to this article can be found online at https://doi.org/10.1016/j.mtbio.2024.101347.

Abbreviations

AD	Alzheimer's disease
CMCDs	metformin carbon dots
NSCs	neural stem cell
Aβ	amyloid beta
DG	dentate gyrus
(BBB)	blood-brain barrier
CDs	Carbon dots
CA	citric acid
DMEM/F12	DMEM/F12-Dulbecco's Modified Eagle Medium
TEM	Transmission electron microscopy
HRTEM	High-resolution TEM
PL,	Photoluminescence
FTIR	Fourier transform infrared
XPS	X-ray photoelectron spectroscopy
HFIP	hexafluoroisopropanol
DMSO	dimethyl sulfoxide
PDL,	poly-D-lysine
Met-CA mix	metformin-citric acid mixture
MWN	Morris water maze

Data availability

Data will be made available on request.

References

[1] 2023 Alzheimer's disease facts and figures, Alzheimers Dement, J. Alzheimers Assoc. 19 (2023) 1598–1695, https://doi.org/10.1002/alz.13016.
[2] Q. Wang, L. Duan, X. Li, Y. Wang, W. Guo, F. Guan, S. Ma, Glucose metabolism, neural cell senescence and Alzheimer's disease, Int. J. Mol. Sci. 23 (2022) 4351, https://doi.org/10.3390/ijms23084351.
[3] D.J. Selkoe, Deciphering the genesis and fate of amyloid beta-protein yields novel therapies for Alzheimer disease, J. Clin. Invest. 110 (2002) 1375–1381, https://doi.org/10.1172/JCI16783.
[4] C. Sharma, S. Kim, Y. Nam, U.J. Jung, S.R. Kim, Mitochondrial dysfunction as a driver of cognitive impairment in Alzheimer's disease, Int. J. Mol. Sci. 22 (2021) 4850, https://doi.org/10.3390/ijms22094850.
[5] W. Liao, J. Xu, B. Li, Y. Ruan, T. Li, J. Liu, Deciphering the roles of metformin in Alzheimer's disease: a snapshot, Front. Pharmacol. 12 (2022), https://doi.org/10.3389/fphar.2021.728315.
[6] B.P. Dave, Y.B. Shah, K.G. Maheshwari, K.A. Mansuri, B.S. Prajapati, H.I. Postwala, M.R. Chorawala, Pathophysiological aspects and therapeutic armamentarium of Alzheimer's disease: recent trends and future development, Cell. Mol. Neurobiol. (2023), https://doi.org/10.1007/s10571-023-01408-7.
[7] P. Ning, Exploring the dual character of metformin in Alzheimer's disease. https://doi.org/10.1016/j.neuropharm.2022.108966, 2022.
[8] G. Kempermann, What is adult hippocampal neurogenesis good for? Front. Neurosci. 16 (2022) 852680 https://doi.org/10.3389/fnins.2022.852680.
[9] J. Shen, D. Wang, X. Wang, S. Gupta, B. Ayloo, S. Wu, P. Prasad, Q. Xiong, J. Xia, S. Ge, Neurovascular coupling in the dentate gyrus regulates adult hippocampal neurogenesis, Neuron 103 (2019) 878–890.e3, https://doi.org/10.1016/j.neuron.2019.05.045.
[10] T.A. Kim, M.D. Syty, K. Wu, S. Ge, Adult hippocampal neurogenesis and its impairment in Alzheimer's disease, Zool. Res. 43 (2022) 481–496, https://doi.org/10.24272/j.issn.2095-8137.2021.479.
[11] K.R. Babcock, J.S. Page, J.R. Fallon, A.E. Webb, Adult hippocampal neurogenesis in aging and Alzheimer's disease, Stem Cell Rep. 16 (2021) 681–693, https://doi.org/10.1016/j.stemcr.2021.01.019.
[12] Q. Zhang, J. Liu, L. Chen, M. Zhang, Promoting endogenous neurogenesis as a treatment for Alzheimer's disease, Mol. Neurobiol. 60 (2023) 1353–1368, https://doi.org/10.1007/s12035-022-03145-2.
[13] P.-C. Chen, X. Han, T.I. Shaw, Y. Fu, H. Sun, M. Niu, Z. Wang, Y. Jiao, B.J. W. Teubner, D. Eddins, L.N. Beloate, B. Bai, J. Mertz, Y. Li, J.-H. Cho, X. Wang, Z. Wu, D. Liu, S. Poudel, Z.-F. Yuan, A. Mancieri, J. Low, H.-M. Lee, M.H. Patton, L. R. Earls, E. Stewart, P. Vogel, Y. Hui, S. Wan, D.A. Bennett, G.E. Serrano, T. G. Beach, M.A. Dyer, R.J. Smeyne, T. Moldoveanu, T. Chen, G. Wu, S. S. Zakharenko, G. Yu, J. Peng, Alzheimer's disease-associated U1 snRNP splicing dysfunction causes neuronal hyperexcitability and cognitive impairment, Nat. Aging 2 (2022) 923–940, https://doi.org/10.1038/s43587-022-00290-0.
[14] K. Pang, R. Jiang, W. Zhang, Z. Yang, L.-L. Li, M. Shimozawa, S. Tambaro, J. Mayer, B. Zhang, M. Li, J. Wang, H. Liu, A. Yang, X. Chen, J. Liu, B. Winblad, H. Han, T. Jiang, W. Wang, P. Nilsson, W. Guo, B. Lu, An App knock-in rat model for Alzheimer's disease exhibiting Aβ and tau pathologies, neuronal death and cognitive impairments, Cell Res. 32 (2022) 157–175, https://doi.org/10.1038/s41422-021-00582-x.
[15] N. Nisa, B. Rasmita, C. Arati, C. Uditraj, R. Siddhartha, R. Dinata, B. Bhanushree, R. M. Bidanchi, B. Manikandan, S.A. Laskar, G. Abinash, B. Pori, V.K. Roy, G. Gurusubramanian, Repurposing of phyto-ligand molecules from the honey bee products for Alzheimer's disease as novel inhibitors of BACE-1: small molecule bioinformatics strategies as amyloid-based therapy, Environ. Sci. Pollut. Res. Int. 30 (2023) 51143–51169, https://doi.org/10.1007/s11356-023-25943-4.
[16] S. Datta, A. Gajbhiye, S. Patil, Pegylated chitosan biodegradable nanoparticles delivery of salvia officinalis and melissa officinalis for enhanced brain targeting, Curr. Nanomedicine 13 (n.d.) 1–13.
[17] M.-R. Du, Q.-Y. Gao, C.-L. Liu, L.-Y. Bai, T. Li, F.-L. Wei, Exploring the pharmacological potential of metformin for neurodegenerative diseases, Front. Aging Neurosci. 14 (2022) 838173, https://doi.org/10.3389/fnagi.2022.838173.
[18] T. Li, Y. Yin, N. Mu, Y. Wang, M. Liu, M. Chen, W. Jiang, L. Yu, Y. Li, H. Ma, Metformin-enhanced cardiac AMP-activated protein kinase/atrogin-1 pathways inhibit charged multivesicular body protein 2B accumulation in ischemia–reperfusion injury, Front. Cell Dev. Biol. 8 (2021) 621509, https://doi.org/10.3389/fcell.2020.621509.
[19] T. Li, R. Providencia, W. Jiang, N. Mu, Y. Wang, X. Li, Y. Yin, M. Liu, L. Yu, C. Gu, A.C.Y. Chang, H. Ma, Association of metformin with the mortality and incidence of cardiovascular events in patients with pre-existing cardiovascular diseases. https://doi.org/10.22541/au.164864421.14975800/v1, 2022.
[20] T. Li, R. Providencia, N. Mu, Y. Yin, M. Chen, Y. Wang, M. Liu, L. Yu, C. Gu, H. Ma, Association of metformin monotherapy or combined therapy with cardiovascular risks in patients with type 2 diabetes mellitus, Cardiovasc. Diabetol. 20 (2021) 30, https://doi.org/10.1186/s12933-020-01202-5.
[21] A. Dihoum, G. Rena, E.R. Pearson, C.C. Lang, I.R. Mordi, Metformin: evidence from preclinical and clinical studies for potential novel applications in cardiovascular disease, Expet Opin. Invest. Drugs 32 (2023) 291–299, https://doi.org/10.1080/13543784.2023.2196010.
[22] Metformin treatment attenuates tau seeding in neuritic plaques - Zhao - 2020 - Alzheimer's & Dementia - Wiley Online Library, (n.d.). https://alz-journals.onlinelibrary.wiley.com/doi/10.1002/alz.041470 (accessed November 12, 2023).
[23] X. Zhu, J. Shen, S. Feng, C. Huang, Z. Liu, Y.E. Sun, H. Liu, Metformin improves cognition of aged mice by promoting cerebral angiogenesis and neurogenesis, Aging 12 (2020) 17845–17862, https://doi.org/10.18632/aging.103693.
[24] X. Ma, W. Xiao, H. Li, P. Pang, F. Xue, L. Wan, L. Pei, H. Yan, Metformin restores hippocampal neurogenesis and learning and memory via regulating gut microbiota in the obese mouse model, Brain Behav. Immun. 95 (2021) 68–83, https://doi.org/10.1016/j.bbi.2021.02.011.
[25] W. Liao, J. Xu, B. Li, Y. Ruan, T. Li, J. Liu, Deciphering the roles of metformin in Alzheimer's disease: a snapshot, Front. Pharmacol. 12 (2021) 728315, https://doi.org/10.3389/fphar.2021.728315.
[26] S.A. Farr, E. Roesler, M.L. Niehoff, D.A. Roby, A. McKee, J.E. Morley, Metformin improves learning and memory in the SAMP8 mouse model of Alzheimer's disease, J. Alzheimers Dis. JAD 68 (2019) 1699–1710, https://doi.org/10.3233/JAD-181240.
[27] S. Rabieipoor, M. Zare, M. Ettcheto, A. Camins, M. Javan, Metformin restores cognitive dysfunction and histopathological deficits in an animal model of sporadic Alzheimer's disease, Heliyon 9 (2023) e17873, https://doi.org/10.1016/j.heliyon.2023.e17873.
[28] Z.H. Houston, J. Bunt, K.-S. Chen, S. Puttick, C.B. Howard, N.L. Fletcher, A. V. Fuchs, J. Cui, Y. Ju, G. Cowin, X. Song, A.W. Boyd, S.M. Mahler, L.J. Richards, F. Caruso, K.J. Thurecht, Understanding the uptake of nanomedicines at different stages of brain cancer using a modular nanocarrier platform and precision

bispecific antibodies, ACS Cent. Sci. 6 (2020) 727–738, https://doi.org/10.1021/acscentsci.9b01299.
[29] Z. Zhang, Y.-A. Lin, S.-Y. Kim, L. Su, J. Liu, R.M. Kannan, S. Kannan, Systemic dendrimer-drug nanomedicines for long-term treatment of mild-moderate cerebral palsy in a rabbit model, J. Neuroinflammation 17 (2020) 319, https://doi.org/10.1186/s12974-020-01984-1.
[30] D. Gonzalez-Carter, X. Liu, T.A. Tockary, A. Dirisala, K. Toh, Y. Anraku, K. Kataoka, Targeting nanoparticles to the brain by exploiting the blood-brain barrier impermeability to selectively label the brain endothelium, Proc. Natl. Acad. Sci. U. S.A. 117 (2020) 19141–19150, https://doi.org/10.1073/pnas.2002016117.
[31] A. Tahmasbi Rad, C.-W. Chen, W. Aresh, Y. Xia, P.-S. Lai, M.-P. Nieh, Combinational effects of active targeting, shape, and enhanced permeability and retention for cancer theranostic nanocarriers, ACS Appl. Mater. Interfaces 11 (2019) 10505–10519, https://doi.org/10.1021/acsami.8b21609.
[32] J. Liu, R. Li, B. Yang, Carbon dots: a new type of carbon-based nanomaterial with wide applications, ACS Cent. Sci. 6 (2020) 2179–2195, https://doi.org/10.1021/acscentsci.0c01306.
[33] B.D. Mansuriya, Z. Altintas, Carbon dots: classification, properties, synthesis, characterization, and applications in health care—an updated review (2018–2021), Nanomaterials 11 (2021) 2525, https://doi.org/10.3390/nano11102525.
[34] E.S. Seven, Y.B. Seven, Y. Zhou, S. Poudel-Sharma, J.J. Diaz-Rucco, E. Kirbas Cilingir, G.S. Mitchell, J.D. Van Dyken, R.M. Leblanc, Crossing the blood–brain barrier with carbon dots: uptake mechanism and in vivo cargo delivery, Nanoscale Adv. 3 (n.d.) 3942–3953. https://doi.org/10.1039/d1na00145k.
[35] E. Kirbas Cilingir, E.S. Seven, Y. Zhou, B.M. Walters, K.J. Mintz, R.R. Pandey, A. H. Wikramanayake, C.C. Chusuei, S. Vanni, R.M. Graham, R.M. Leblanc, Metformin derived carbon dots: highly biocompatible fluorescent nanomaterials as mitochondrial targeting and blood-brain barrier penetrating biomarkers, J. Colloid Interface Sci. 592 (2021) 485–497, https://doi.org/10.1016/j.jcis.2021.02.058.
[36] B. Anand, Q. Wu, M. Nakhaei-Nejad, G. Karthivashan, L. Dorosh, S. Amidian, A. Dahal, X. Li, M. Stepanova, H. Wille, F. Giuliani, S. Kar, Significance of native PLGA nanoparticles in the treatment of Alzheimer's disease pathology, Bioact. Mater. 17 (2022) 506–525, https://doi.org/10.1016/j.bioactmat.2022.05.030.
[37] S.K.L. Rompicherla, K. Arumugam, S.L. Bojja, N. Kumar, C.M. Rao, Pharmacokinetic and pharmacodynamic evaluation of nasal liposome and nanoparticle based rivastigmine formulations in acute and chronic models of Alzheimer's disease, Naunyn-Schmiedeberg's Arch. Pharmacol. 394 (2021) 1737–1755, https://doi.org/10.1007/s00210-021-02096-0.
[38] Y. Zhou, P.Y. Liyanage, D. Devadoss, L.R. Rios Guevara, L. Cheng, R.M. Graham, H. S. Chand, A.O. Al-Youbi, A.S. Bashammakh, M.S. El-Shahawi, R.M. Leblanc, Nontoxic amphiphilic carbon dots as promising drug nanocarriers across the blood–brain barrier and inhibitors of β-amyloid, Nanoscale 11 (2019) 22387–22397, https://doi.org/10.1039/C9NR08194A.
[39] M.Z. Zhong, Updates on mouse models of Alzheimer's disease. Sex Differ, 2024.
[40] E. Salta, O. Lazarov, C.P. Fitzsimons, R. Tanzi, P.J. Lucassen, S.H. Choi, Adult hippocampal neurogenesis in Alzheimer's disease: a roadmap to clinical relevance, Cell Stem Cell 30 (2023) 120–136, https://doi.org/10.1016/j.stem.2023.01.002.
[41] M.L. Liu, B.B. Chen, C.M. Li, C.Z. Huang, Carbon dots: synthesis, formation mechanism, fluorescence origin and sensing applications, Green Chem. 21 (2019) 449–471, https://doi.org/10.1039/C8GC02736F.
[42] T.V. de Medeiros, J. Manioudakis, F. Noun, J.-R. Macairan, F. Victoria, R. Naccache, Microwave-assisted synthesis of carbon dots and their applications, J. Mater. Chem. C 7 (2019) 7175–7195, https://doi.org/10.1039/C9TC01640F.
[43] P.Y. Liyanage, R.M. Graham, R.R. Pandey, C.C. Chusuei, K.J. Mintz, Y. Zhou, J. K. Harper, W. Wu, A.H. Wikramanayake, S. Vanni, R.M. Leblanc, Carbon nitride dots: a selective bioimaging nanomaterial, Bioconjugate Chem. 30 (2019) 111–123, https://doi.org/10.1021/acs.bioconjchem.8b00784.
[44] D. Zhou, P. Jing, Y. Wang, Y. Zhai, D. Li, Y. Xiong, A.V. Baranov, S. Qu, A. L. Rogach, Carbon dots produced *via* space-confined vacuum heating: maintaining efficient luminescence in both dispersed and aggregated states, Nanoscale Horiz 4 (2019) 388–395, https://doi.org/10.1039/C8NH00247A.
[45] M.H. Park, K.H. Park, B.J. Choi, W.H. Han, H.J. Yoon, H.Y. Jung, J. Lee, I.-S. Song, D.Y. Lim, M.-K. Choi, Y.-H. Lee, C.-M. Park, M. Wang, J. Jo, H.-J. Kim, S.H. Kim, E. H. Schuchman, H.K. Jin, J. Bae, Discovery of a dual-action small molecule that improves neuropathological features of Alzheimer's disease mice, Proc. Natl. Acad. Sci. USA 119 (2022) e2115082119, https://doi.org/10.1073/pnas.2115082119.
[46] O. Rybachuk, O. Kopach, T. Pivneva, V. Kyryk, Isolation of neural stem cells from the embryonic mouse Hippocampus for in vitro growth or engraftment into a host tissue, BIO-Protoc 9 (2019), https://doi.org/10.21769/BioProtoc.3165.
[47] C. Vinel, G. Rosser, L. Guglielmi, M. Constantinou, N. Pomella, X. Zhang, J.R. Boot, T.A. Jones, T.O. Millner, A.A. Dumas, V. Rakyan, J. Rees, J.L. Thompson, J. Vuononvirta, S. Nadkarni, T. El Assan, N. Aley, Y.-Y. Lin, P. Liu, S. Nelander, D. Sheer, C.L.R. Merry, F. Marelli-Berg, S. Brandner, S. Marino, Comparative epigenetic analysis of tumour initiating cells and syngeneic EPSC-derived neural stem cells in glioblastoma, Nat. Commun. 12 (2021) 6130, https://doi.org/10.1038/s41467-021-26297-6.
[48] H. Yang, Y. Su, Z. Sun, B. Ma, F. Liu, Y. Kong, C. Sun, B. Li, Y. Sang, S. Wang, G. Li, J. Qiu, C. Liu, Z. Geng, H. Liu, Gold nanostrip array-mediated wireless electrical stimulation for accelerating functional neuronal differentiation, Adv. Sci. 9 (2022) 2202376, https://doi.org/10.1002/advs.202202376.
[49] L. Ye, H. Ji, J. Liu, C. Tu, M. Kappl, K. Koynov, J. Vogt, H. Butt, Carbon nanotube–hydrogel composites facilitate neuronal differentiation while maintaining homeostasis of network activity, Adv. Mater. 33 (2021) 2102981, https://doi.org/10.1002/adma.202102981.
[50] C. Syal, J. Kosaraju, L. Hamilton, A. Aumont, A. Chu, S.N. Sarma, J. Thomas, M. Seegobin, F.J. Dilworth, L. He, F.E. Wondisford, R. Zimmermann, M. Parent, K. Fernandes, J. Wang, Dysregulated expression of monoacylglycerol lipase is a marker for anti-diabetic drug metformin-targeted therapy to correct impaired neurogenesis and spatial memory in Alzheimer's disease, Theranostics 10 (2020) 6337–6360, https://doi.org/10.7150/thno.44962.
[51] G. Cheung, D. Bataveljic, J. Visser, N. Kumar, J. Moulard, G. Dallérac, D. Mozheiko, A. Rollenhagen, P. Ezan, C. Mongin, O. Chever, A.-P. Bemelmans, J. Lübke, I. Leray, N. Rouach, Physiological synaptic activity and recognition memory require astroglial glutamine, Nat. Commun. 13 (2022) 753, https://doi.org/10.1038/s41467-022-28331-7.
[52] S. Ziegler-Waldkirch, M. Friesen, D. Loreth, J.-F. Sauer, S. Kemna, A. Hilse, D. Erny, C. Helm, P. d'Errico, M. Prinz, M. Bartos, M. Meyer-Luehmann, Seed-induced Aβ deposition alters neuronal function and impairs olfaction in a mouse model of Alzheimer's disease, Mol. Psychiatr. 27 (2022) 4274–4284, https://doi.org/10.1038/s41380-022-01686-5.
[53] D. Lecca, Y.J. Jung, M.T. Scerba, I. Hwang, Y.K. Kim, S. Kim, S. Modrow, D. Tweedie, S. Hsueh, D. Liu, W. Luo, E. Glotfelty, Y. Li, J. Wang, Y. Luo, B. J. Hoffer, D.S. Kim, R.A. McDevitt, N.H. Greig, Role of chronic neuroinflammation in neuroplasticity and cognitive function: a hypothesis, Alzheimers Dement 18 (2022) 2327–2340, https://doi.org/10.1002/alz.12610.
[54] F. Leng, P. Edison, Neuroinflammation and microglial activation in Alzheimer disease: where do we go from here? Nat. Rev. Neurol. 17 (2021) 157–172, https://doi.org/10.1038/s41582-020-00435-y.